Journal of Power Sources 196 (2011) 5155–5167

Contents lists available at ScienceDirect

Journal of Power Sources

journal homepage: www.elsevier.com/locate/jpowsour

Influence of carbons on the structure of the negative active material of lead-acid batteries and on battery performance

D. Pavlov*, P. Nikolov, T. Rogachev

Institute of Electrochemistry and Energy Systems (IEES), Bulgarian Academy of Sciences, Acad. Georgi Bonchev, Block 10, Sofia 1113, Bulgaria

ARTICLE INFO

Article history:
Received 16 November 2010
Received in revised form
22 December 2010
Accepted 2 February 2011
Available online 12 February 2011

Keywords:
Lead-acid battery
Negative plate charge acceptance
Carbon additive to lead battery plate
Structure of negative active material
Activated carbon in lead battery plates
Carbon black in lead battery plates

ABSTRACT

It has been established that addition of carbon additives to the lead negative active material (NAM) of lead-acid batteries increase battery charge acceptance in hybrid electric vehicle mode of operation. The present work studies three types of activated carbons and two types of carbon blacks with the aim to evaluate their efficiency in improving the charge acceptance of lead-acid batteries. It has been established that the size of carbon particles and their affinity to lead are essential. If carbon particles are of nanosizes, they are incorporated into the bulk of the skeleton branches of NAM and may thus increase the latter's ohmic resistance. Their content in NAM should not exceed 0.2–0.5 wt.%. At this loading level, carbon grains are adsorbed only on the surface of NAM contributing to the increase of its specific surface area and thus improving its charge acceptance. When carbon particles are of micron sizes and have high affinity to lead, they are integrated into the skeleton structure of NAM as a structural component and act as super-capacitors, i.e. electric charges are concentrated in them and then the current is distributed along the adjacent branches of the lead skeleton with the lowest ohmic resistance. This eventually improves the charge acceptance of the negative battery plates.

1. Introduction

Batteries in hybrid electric vehicles operate from partial state of charge and experience short charge and discharge pulses with high currents. The negative active material has low specific surface area, which results in high current density, low charge acceptance and progressive sulfation of the negative plates. It is these deficiencies of the negative plates that limit the wider use of lead-acid batteries for electric vehicle applications. Methods have been searched to improve the charge acceptance of the negative plates in EV cycling duties.

Nakamura, Shiomi and co-authors [1,2] have established that introduction of carbon black to the negative active material retards substantially the sulfation of the negative plates during the simulated high-rate partial-state-of-charge (HRPSoC) test of batteries for hybrid electric vehicle (HEV) applications. Several mechanisms of the effect of carbons on the processes at the negative plates of lead-acid batteries operated under HRPSoC conditions have been proposed. Moseley et al. [3] have summarized the hypotheses proposed in the literature for the action of carbons on the HRPSoC performance of the batteries as follows: (a) carbon enhances the overall conductivity of NAM [1,4]; (b) carbon facilitates the formation of small isolated $PbSO_4$ particles easy to dissolve and restricts $PbSO_4$ crystal growth [2]; (c) some carbon forms contain impurities which impede the reaction of hydrogen evolution and hence improve the efficiency of charge [5,6]; (d) carbon acts as an electro-osmotic pump that facilitates acid diffusion in the inner NAM volume at the high rates of charge and discharge [3]; high-surface-area carbon black particles have a supercapacitive effect in NAM [7]. A comprehensive survey of the influence of a wide spectrum of carbon materials introduced as additives to NAM on the HRPSoC cycling performance is provided in Ref. [8].

On charging of valve-regulated lead-acid batteries (VRLAB) "a closed oxygen cycle" may operate. Oxygen is evolved at the positive plates, diffuses to the negatives and is reduced there forming water. When carbon is added to the negative active material it may be oxidized by the evolved oxygen and thus its beneficial effect on the charge acceptance of the negative plates may be suppressed or even eliminated altogether. Hence, it is very important to find such carbon material(s) that would be more resistant to oxidation. Evolution of oxygen commences at a low rate when the battery reaches 75% state-of-charge (SOC). As a rule, batteries in hybrid electric vehicle applications operate between 80 and 30% SOC. When the battery is charged to above 75% SOC, the effect of the reactions of the closed oxygen cycle should be accounted for. These reactions have been discussed in detail by Bullock in Ref. [9].

* Corresponding author. Tel.: +359 2 971 00 83; fax: +359 2 873 15 52.
E-mail address: dpavlov@labatscience.com (D. Pavlov).

0378-7753/$ – see front matter © 2011 Elsevier B.V. All rights reserved.
doi:10.1016/j.jpowsour.2011.02.014

Table 1
Summary and specific characteristics of the selected additives used in this study.

Product	Manufacturer	Type of material	Signature	Specific characteristics according manufacturer	
				Particle size	BET surface
SO-15A	TDA Research Inc.	Activated carbon	TDA	<44 μm	1615 $m^2 g^{-1}$
Purified WV-E 105	Mead Westvaco Corp.	Activated carbon	MWV	8.7 μm	2415 $m^2 g^{-1}$
NORIT AZO	Norit Activated Carbon	Activated carbon	NAZ	<100 μm	635 $m^2 g^{-1}$
PRINTEX® 90	EVONIK INDUSTRIE	Carbon black	PR90	14 nm	300 $m^2 g^{-1}$
PRINTEX® U	EVONIK INDUSTRIE	Carbon black	PRU	25 nm	100 $m^2 g^{-1}$
$BaSO_4$	Sachtleben Chemie	Crystal powder	$BaSO_4$		

In the course of work within a research project sponsored by the advanced lead-acid battery consortium (ALABC), we have established that, during cycling of cells under HRPSoC conditions, the electrochemical reactions of charge at the negative plates proceed not only on the lead surface, but on the surface of the carbon phase as well [10,11]. Thus, carbon particles in NAM are involved in the charge process. We called this mechanism "parallel electrochemical mechanism of charge" [10]. The currents flowing through the Pb and C surfaces will depend on the properties and electrochemical activity of the two interfaces: Pb/H_2SO_4 and $carbon/H_2SO_4$.

Analyzing the parallel mechanism of charge we have come to the conclusion that carbons must be included in the structure of the negative active material (NAM) to be able to take part in the electrochemical reactions. And their inclusion in the NAM structure will depend on the affinity of the carbon additive to lead, on carbon particle size and on the type and structure of the Pb active mass.

The aim of the present investigation is to find out where and how are carbon particles incorporated in the structure of the negative active mass, and what is the impact of the respective NAM structures on battery performance in the HRPSoC duty.

2. Experimental

2.1. Carbon forms added to the negative active material

We studied the influence of the following additives to the negative active material: three types of activated carbons, two types of carbon blacks of the Printex series, and barium sulfate. No lignosulfonate was added to the negative pastes in these experiments. A summary of the types of additives used in this study is presented in Table 1.

The effect of five different concentrations of each carbon type on the parameters of the lead-acid cell was evaluated at three $BaSO_4$ concentrations with the aim to determine the optimum carbon and $BaSO_4$ loading levels that have the most beneficial effect on charge acceptance in the HRPSoC cycling duty.

2.2. Negative plate preparation

The negative pastes for these experiments were prepared using H_2SO_4 (1.4 sp.gr.) and leady oxide (LO) in 4.5 wt.% ratio. The degree of oxidation of the LO was 76%. Barton oxide from the Bulgarian battery plant MONBAT was used. Barium sulfate was added in three different concentrations: 0.4 wt.%, 0.8 wt.% and 1.2 wt.%, and the carbon content was varied from 0.2 wt.% to 2.0 wt.%. A control batch of paste without carbon was also prepared and used for assembling a reference cell. A total of 21 different paste batches were prepared. These pastes were used for production of negative plates for the test cells. The grids were cast from Pb–0.05%Ca–1.1%Sn alloy.

All plates were formed under identical conditions: in H_2SO_4 (1.06 sp.gr.) for 18 h, employing a formation algorithm developed in this laboratory. The formation process was completed with twice higher quantity of electricity than the theoretical capacity of the cells. After formation, samples of the negative active material were characterized by XRD, chemical analysis, BET surface measurements, mercury porosimetry and SEM examinations.

The influence of carbon and $BaSO_4$ additives on the performance of lead-acid cells was studied using 2 V/4.5 Ah cells analogous to those described in Ref. [10]. Small sized plates were used to rule out the influence of plate size on cell performance as well as of electrolyte stratification in the cell. The test cells comprised two negative plates and three oversized positive plates. 3 mm thick AGM separator was used under 20% compression. The HRPSoC cycling test profile comprised charge and discharge pulses at 2*C* current rate and pulse duration of 60 s. This type of test is employed in many ALABC projects and is discussed in more detail in Ref. [10].

3. Experimental results and discussion

3.1. Influence of carbons and $BaSO_4$ on the macrostructure of NAM

The macrostructure of NAM was characterized in terms of: median pore radius, specific surface area and overall organization of the crystal formations in NAM established by SEM examinations.

Fig. 1 shows the changes in median pore radius of NAM as a function of carbon content, at three different concentrations of $BaSO_4$. The results evidence that Printex® 90 carbon black (PR90), added in concentrations over 0.2 wt.%, and Mead Wesvaco activated carbon (MWV) up to 1.0 wt.%, reduce the median pore radius of NAM down to 1 μm. With increase of the content of TDA SO-15A activated carbon (TDA) the median radius diminishes to 2 μm. Higher loads (>0.5 wt.%) of the Norit AZO activated carbon (NAZ) lead to increase of the median pore radius from 7 to 10 μm.

These results indicate clearly that carbon additives alter the macrostructure of NAM, especially at loading levels equal to or higher than 0.5 wt.%. And NAM macro-structure could be changed only if carbon particles are incorporated in it. This influence should be taken into account because it affects the ion diffusion processes in the plate.

Fig. 2 presents the correlations between the specific surface area of NAM and carbon content. All investigated additives contribute to increase of the specific surface area of NAM with increase of their loading levels. This increase is most pronounced with TDA activated carbon at 2.0 wt.% loading level (25 $m^2 g^{-1}$). NAZ activated carbon, at 2.0 wt.% concentration, increases NAM surface area up to 10 $m^2 g^{-1}$, while PR90 carbon black has the weakest effect. Barium sulfate exerts a certain influence on the specific surface of NAM only when in combination with MWV or PR90 carbons, and at high concentrations of both additives.

Based on the above experimental results (Figs. 1 and 2) we can draw the following conclusion: if carbon particles change the median pore radius of NAM, then they must be incorporated into the macrostructure of the negative active mass, thus changing its porous system and increasing its specific surface area.

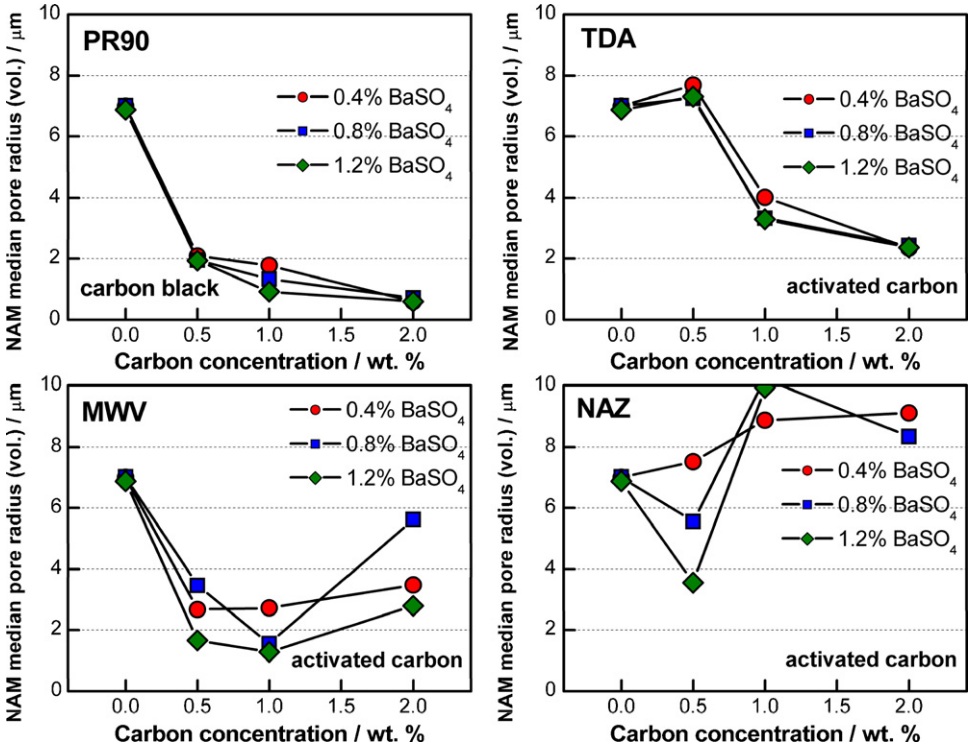

Fig. 1. Influence of carbon and $BaSO_4$ concentrations on the median pore radius of NAM.

3.2. *Influence of carbons and $BaSO_4$ on the microstructure of NAM*

Fig. 3 presents SEM images of the microstructure of NAM with carbon and $BaSO_4$ additives. These images feature a lead skeleton or network. The skeleton in the left hand micrograph (Fig. 3a) consists of numerous interconnected branches of different thickness and various lengths. The right hand micrograph (Fig. 3b) shows spheroidal lead grains also interconnected in a network.

During discharge, parts of the lead skeleton are oxidized to $PbSO_4$ and they determine the capacity of the negative plates. The skeleton is then restored during re-charge. These parts form the energetic structure of NAM. The remaining non-oxidized part of the lead skeleton plays the role of current-conducting structure. It conducts the electric current from the plate grid to each point of the active mass even when the plate is being discharged.

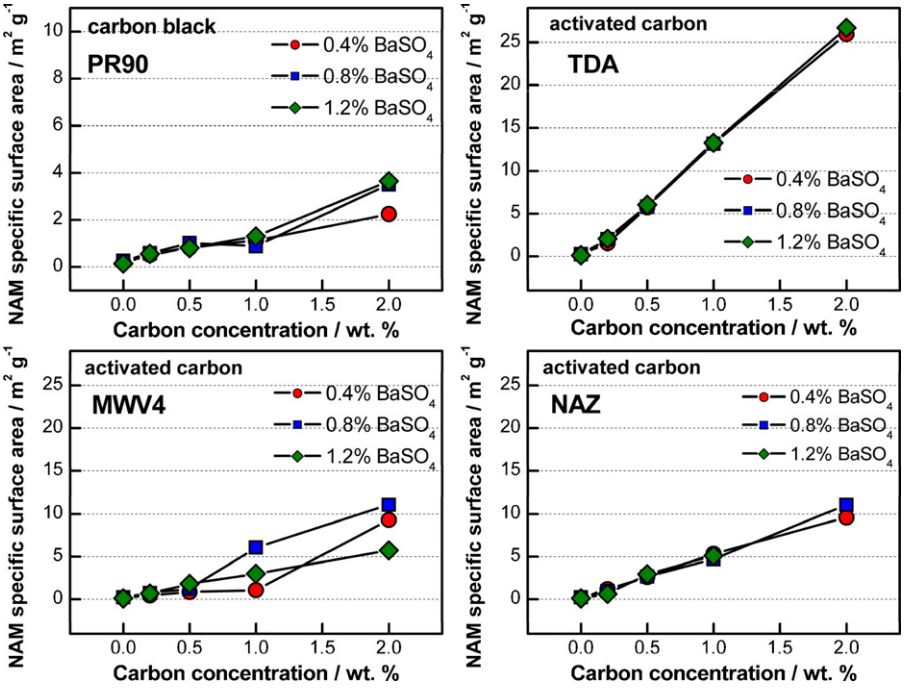

Fig. 2. Influence of carbon and $BaSO_4$ concentrations on the specific surface area of NAM.

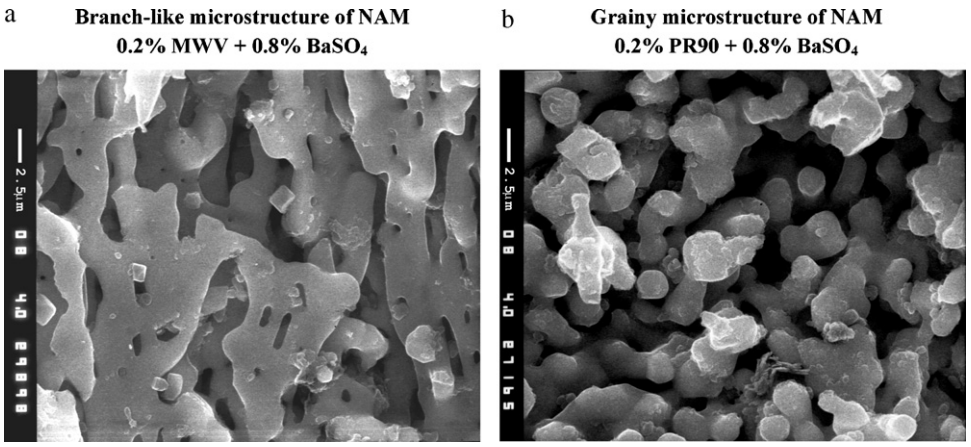

Fig. 3. Microstructure of NAM with 0.8 wt.% $BaSO_4$ and (a) 0.2 wt.% MWV activated carbon, or (b) 0.2 wt.% Printex® 90 carbon black.

The SEM micrographs in Fig. 4 show $BaSO_4$ particles (Fig. 4a) and their location in the structure of NAM with only barium sulfate added (Fig. 4b). Barium sulfate particles are mostly adsorbed at the sites of contact between the Pb particles. These are the sites in the NAM structure with the highest concentration of defects, causing higher concentration of structural energy which goes for the adsorption of $BaSO_4$ particles.

3.3. Inclusion of carbon particles in the structure of the negative active mass

Fig. 5 presents SEM micrographs of Printex® U (PRU) carbon black particles. The two SEM images evidence that PRU carbon black particles are fine grains of nanometer size, which are interconnected in porous formations (aggregates). Due to friction between the particles during the process of paste preparation, these formations have fallen apart to separate grains or small groups of grains.

Let us now see how does the structure of the negative active mass look like when it contains both $BaSO_4$ and carbon black additives. Fig. 6 shows SEM images of NAM with 0.8 wt.% $BaSO_4$ and two different concentrations of PRU carbon black. The carbon black particles are adsorbed on the lead surface and it is strongly folded. The surface area of NAM is increased, thus providing larger surface for the electrochemical reactions to proceed.

As PRU particles adsorb well onto the lead surface, this means that they have high affinity to lead. The question arises logically:

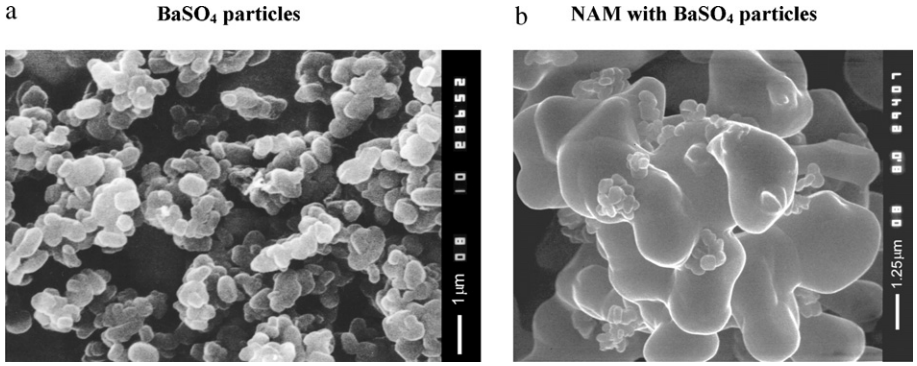

Fig. 4. (a) SEM images of the microstructure of $BaSO_4$ particles; (b) $BaSO_4$ particles adsorbed on NAM surface. They are embedded mainly at the sites of contact between the Pb particles of NAM.

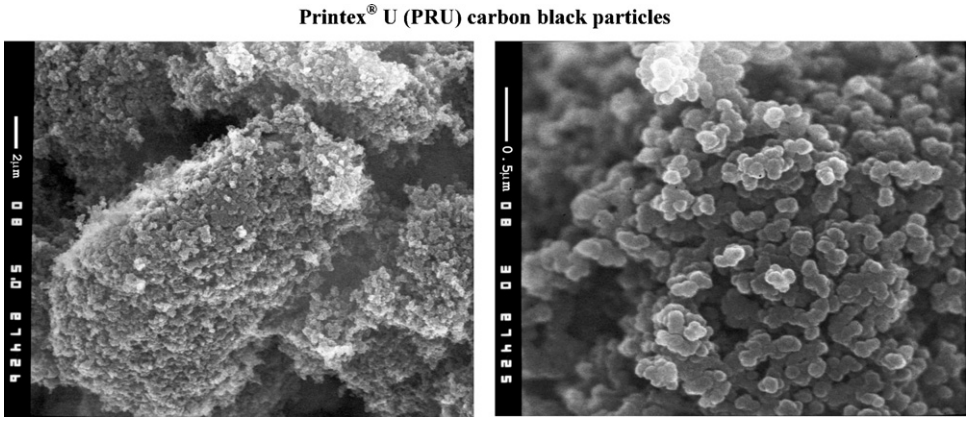

Fig. 5. Microstructure of Printex® U carbon black particles and aggregates.

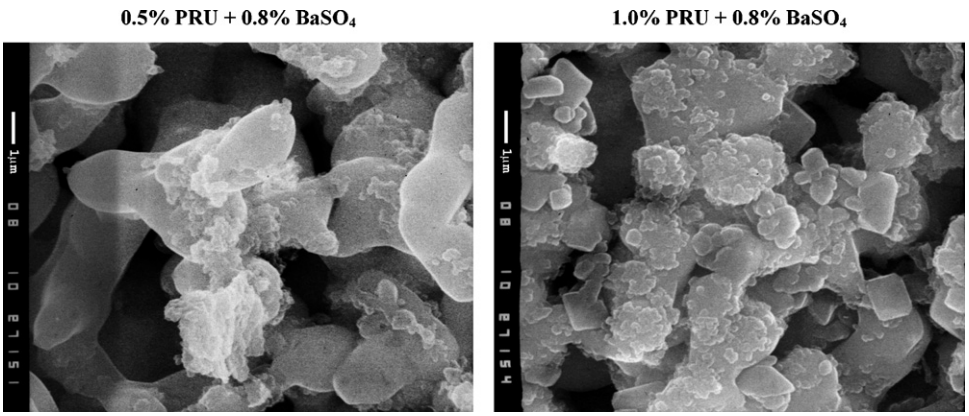

Fig. 6. Microstructure of NAM with 0.8 wt.% $BaSO_4$ and (a) 0.5 wt.% Printex® U carbon black, or (b) 1.0 wt.% Printex® U carbon black.

are these carbon grains adsorbed on the surface of NAM only or are they incorporated into the bulk of the lead skeleton branches?

In order to find the answer to this question, cells with negative plates containing 0.2 wt.%, 1.0 wt.% or 2.0 wt.% PRU carbon black were discharged down to 100% DOD and samples of the active mass were examined by scanning electron microscopy. The obtained SEM micrographs of samples of the discharged active masses are presented in Fig. 7. With increase of the content of PRU carbon black the latter is involved in the growth of the $PbSO_4$ crystals. While at 0.2 wt.% PRU level the $PbSO_4$ crystals have well shaped crystal faces and edges, at the higher concentration of 2.0 wt.% the $PbSO_4$ crystals are rounded due to the embedded carbon particles. The latter create defects in the crystal lattice of $PbSO_4$ which would enhance the solubility of the lead sulfate and thus improve the efficiency of charging with high currents.

In an attempt to examine the structure of the bulk (interior) of the lead skeleton branches after discharge, the $PbSO_4$ crystals were dissolved in ammonium acetate. Fig. 8 presents micrographs of the lead skeleton that has remained after dissolution of the $PbSO_4$ phase. The nature of this skeleton strongly depends on the concentration of the carbon particles. At 0.2 wt.% PRU, almost no carbon grains can be distinguished in the bulk of the skeleton, whereas at higher PRU concentrations (1.0 wt.%, and especially 2.0 wt.%), the skeleton is strongly folded. This is a clear indication that carbon grains are incorporated in the bulk of the lead skeleton branches. The extent of their inclusion in the bulk of the lead skeleton depends on the concentration of carbon blacks in NAM. Obviously, this will have an impact on the reversibility of the processes during HRPSoC cycling.

The inclusion of the PRU carbon grains in the bulk of the lead skeleton branches indicates that this carbon black type has high affinity to lead. During formation of the negative active material, the carbon particles are adsorbed on the lead surface of the growing lead branch. As these particles are electroconductive, the electrochemical reaction of lead ion reduction proceeds on their surface. The newly formed lead surrounds the carbon grain and thus the latter is incorporated into the bulk of the lead branch of NAM skeleton. Hence, for the carbon grains to be incorporated into the bulk of the skeleton branches they should meet the following two requirements:

(a) carbon particles should have high affinity to lead, be electroconductive and electrochemically active;
(b) carbon particles should have a volume (size) considerably smaller than the cross-section of the lead branches of NAM skeleton.

3.4. Influence of Printex® 90 carbon black and $BaSO_4$ concentrations on the HRPSoC cycle life and capacity of the cells

The effect of carbon black additives on cell performance under simulated HRPSoC conditions was tested using a simplified profile imitating the micro-hybrid driving mode. The HRPSoC cycling test profile comprised charge and discharge pulses at 2*C* current rate and pulse duration of 60 s. During these tests the negative plates were cycled between 50 and 53% SoC. The cell voltage was measured at the end of the charge and discharge pulses and the test was stopped when the end-of-discharge voltage fell down to 1.83 V or when the upper end-of-charge voltage limit of 2.83 V was reached. The above described cycling steps comprise one cycle-set of the test. On completion of this cycle set, the capacity of the cells was determined and a new cycle set followed. We assume that the cells have reached their end-of-life when they fail to complete 4000 cycles within one cycle set or when their capacity drops down below 70% of the nominal capacity.

Fig. 9 illustrates the correlations between the number of completed HRPSoC cycles and the content of Printex® 90 (PR90) carbon black in NAM for three different concentrations of $BaSO_4$. As evident from these data, the cells with 0.4 wt.% $BaSO_4$ and 0.2 wt.% PR90 carbon in NAM complete the maximum number of cycles (14,000) within the first cycle set. With increase of the carbon content, the number of completed cycles is sustained between 5000 and 7000 in the first cycle set, but then decreases notably during the second cycle set of the HRPSoC test and the cells reach their end-of-life during the third cycle set.

When the concentration of $BaSO_4$ is increased to 0.8 wt.%, the cells complete about 5000 cycles per cycle set at carbon concentrations of up to 1.0 wt.%. At 2.0 wt.% PR90 loading level, the cells complete less cycles during the first cycle set as compared to the cells with lower carbon content. When added in high concentrations to NAM, $BaSO_4$ and PR90 carbon black seem to suppress each other's positive effect and eventually reduce the number of completed HRPSoC cycles. This adverse effect of $BaSO_4$ is most pronounced when its content in NAM is increased to 1.2 wt.%. At this $BaSO_4$ concentration, only the cells with 0.5 wt.% or 1.0 wt.% PR90 complete more than 4000 cycles in the first and second cycle sets.

The behavior of the cell capacity after each cycle set follows a different pattern. The initial capacity of all cells is higher than the nominal value. The only exceptions are the cells with 0.8 wt.% or 1.2 wt.% $BaSO_4$ and 2.0 wt.% PR90. At 0.4 wt.% or 0.8 wt.% $BaSO_4$ concentration and low PR90 content (0.2 wt.%), the capacity of the cells after each HRPSoC cycle set is lower than the nominal capacity, but it increases with increase of the carbon content in NAM. As a

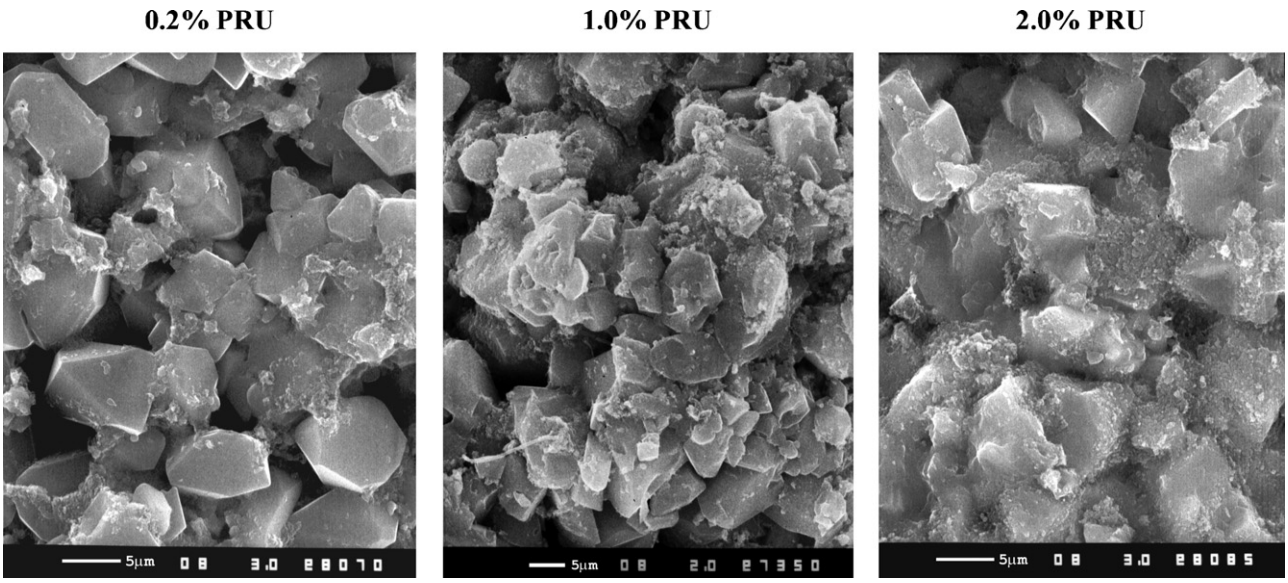

Fig. 7. Microstructure of NAM with different Printex® U carbon black contents after deep discharge (100% DOD) of the negative plates.

whole, the capacity of all cells declines after each subsequent cycle set, yet the cycle life is not limited by the capacity but rather by the number of completed HRPSoC cycles per cycle set.

The above described behavior of cells with Printex® 90 carbon black in NAM can be related to the incorporation of the carbon grains in the bulk of the lead skeleton, whereby they increase its electric resistance and hence reduce the number of completed cycles at high current rate. When present in small quantities in NAM, PR90 carbon particles are adsorbed on the surface of the skeleton only, thus increasing the electrochemically active surface of NAM, which leads eventually to better cycleability at high currents as in this case carbon particles do not increase the ohmic resistance of the NAM skeleton. With increase of the PR90 load in NAM the carbon particles are incorporated into the bulk of the skeleton branches and probably alter their electrical and mechanical properties.

The cells were re-charged to 100% SOC after each cycle set and their capacity was determined. Then, they were discharged to 50% SOC and the next cycle set followed. As evident from Fig. 9 the number of completed cycles decreases with each subsequent cycle set. This decrease is probably a result of the oxidation of carbon by the evolved oxygen during the full re-charge of the cells after each cycle set.

The possible influence of another phenomenon on the observed decline in cycle life within each subsequent cycle set should also be taken into account, namely the partial sulfation of the negative plates. Recrystallization of lead sulfate proceeds during cell cycling and the obtained big $PbSO_4$ crystals do not take part in the reactions during the subsequent cycle set, thus reducing the total number of completed HRPSoC cycles.

Probably, both above described processes take place at the negative plates on HRPSoC cycling, but the impact of each of these processes depends on the rate of oxidation of the carbon added to the negative active material as well as on the $PbSO_4$ recrystallization rate and the morphology of the lead and lead sulfate crystals formed.

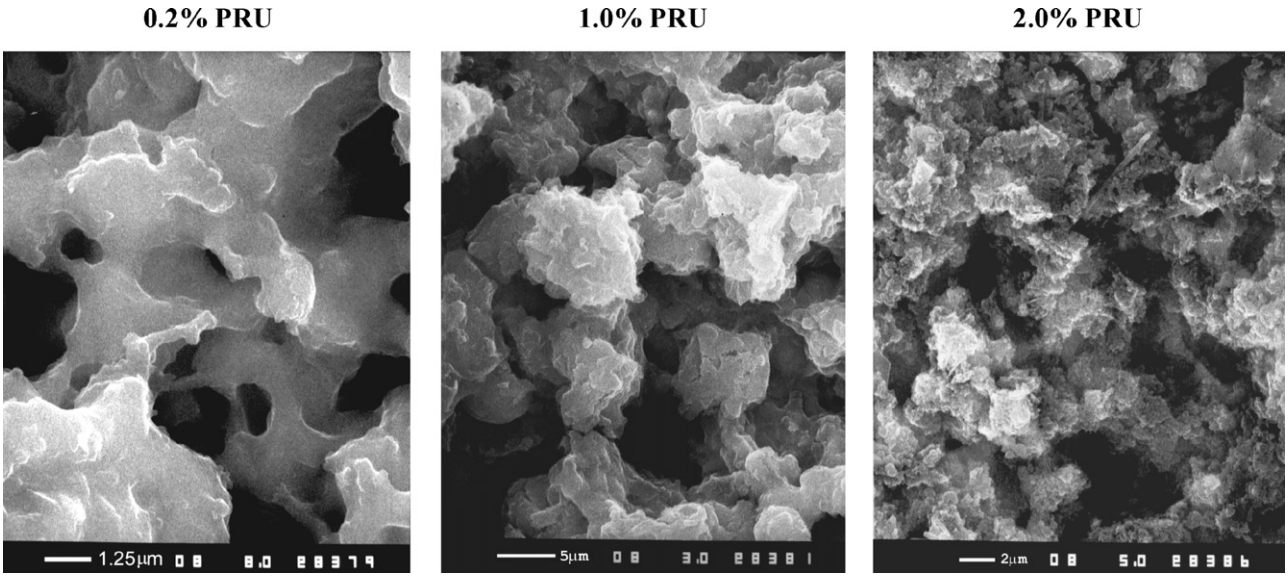

Fig. 8. Microstructure of parts of the inner volume of the current conducting branches of NAM lead skeleton after dissolution of the $PbSO_4$ phase. NAM contains 0.2 wt.%, 1.0 wt.% or 2.0% Printex® U carbon black.

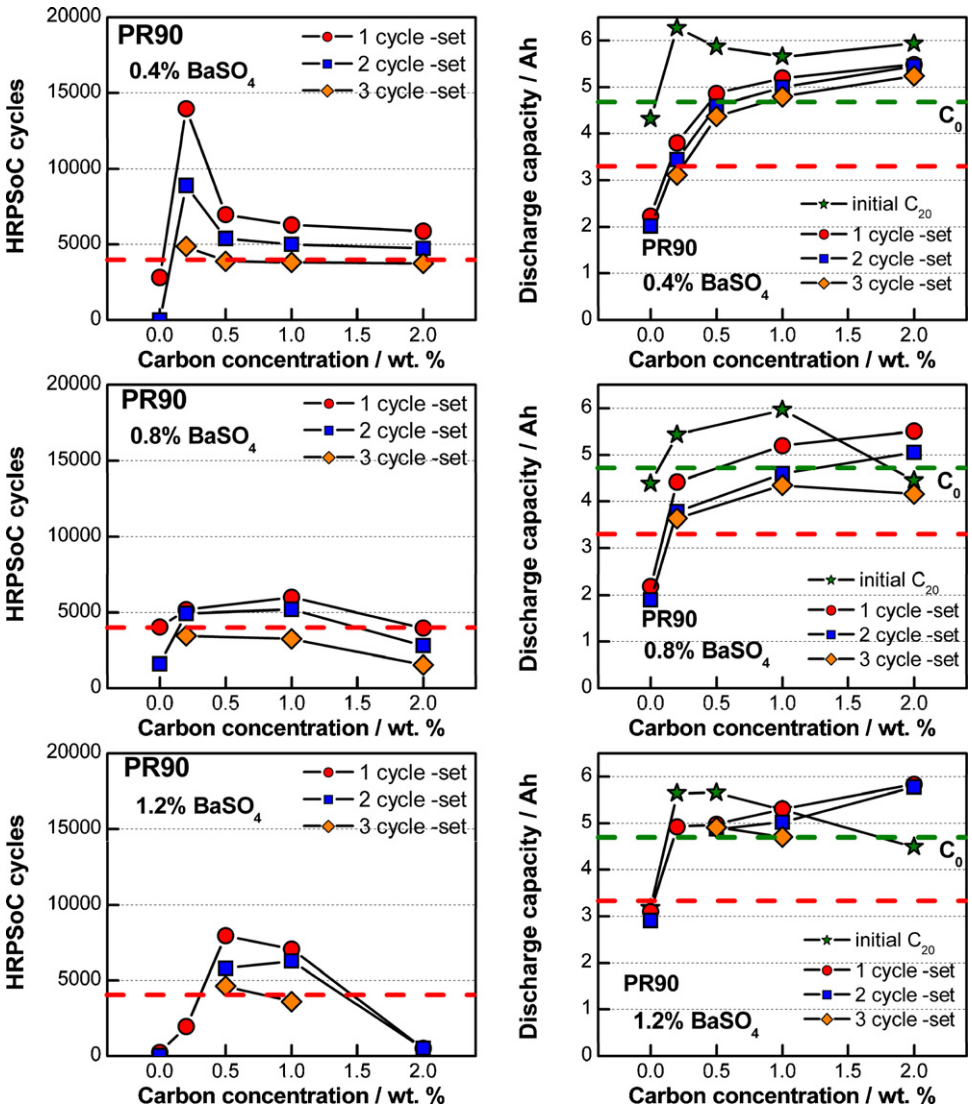

Fig. 9. Influence of Printex® 90 carbon black and $BaSO_4$ concentrations on cell capacity and cycle life during HRPSoC cycling.

3.5. Influence of activated carbons (NAZ, MWV and TDA) on the structure and electrochemical properties of NAM and on the HRPSoC cycle life of lead-acid cells

3.5.1. Effects of Norit AZO activated carbon

SEM micrographs of Norit AZO (NAZ) activated carbon particles are given in Fig. 10. There is a variety of carbon particles of different sizes varying within the micron and down to the sub-micron range. These particles differ in shape, too, the elongated shape being the predominating one.

The structure of NAM with incorporated NAZ carbon particles is presented in Fig. 11. The SEM images show that the NAZ activated carbon particles are included in the lead active mass, but the contact with it is not very "intimate". They look rather like some foreign

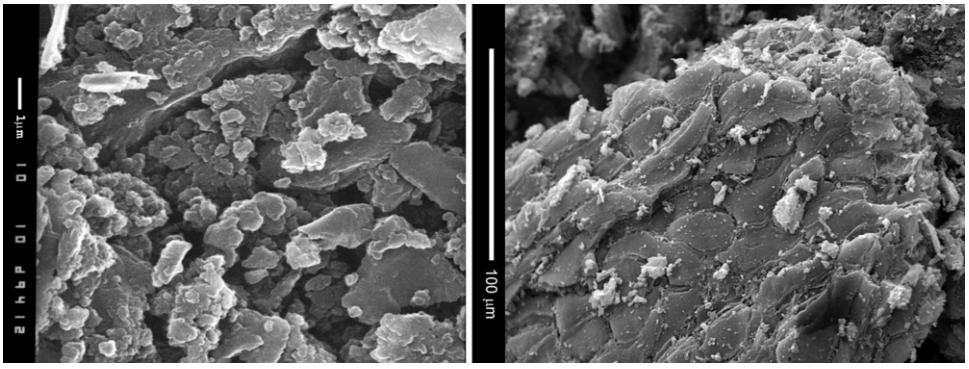

Fig. 10. Microstructure of Norit AZO activated carbon particles.

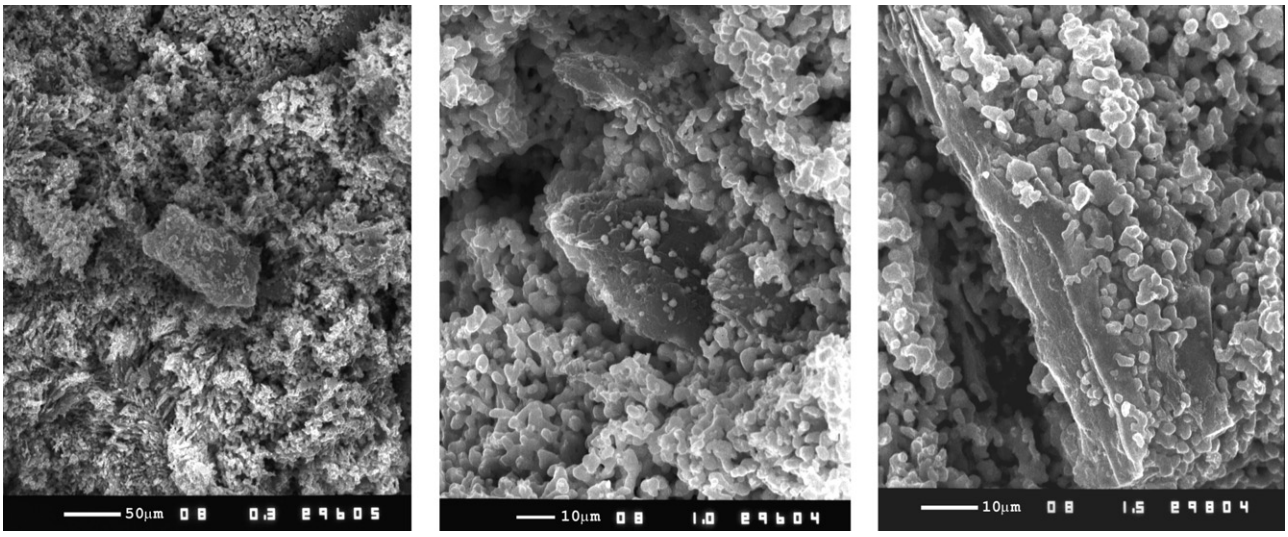

Fig. 11. Microstructure of NAM with incorporated Norit AZO activated carbon particles.

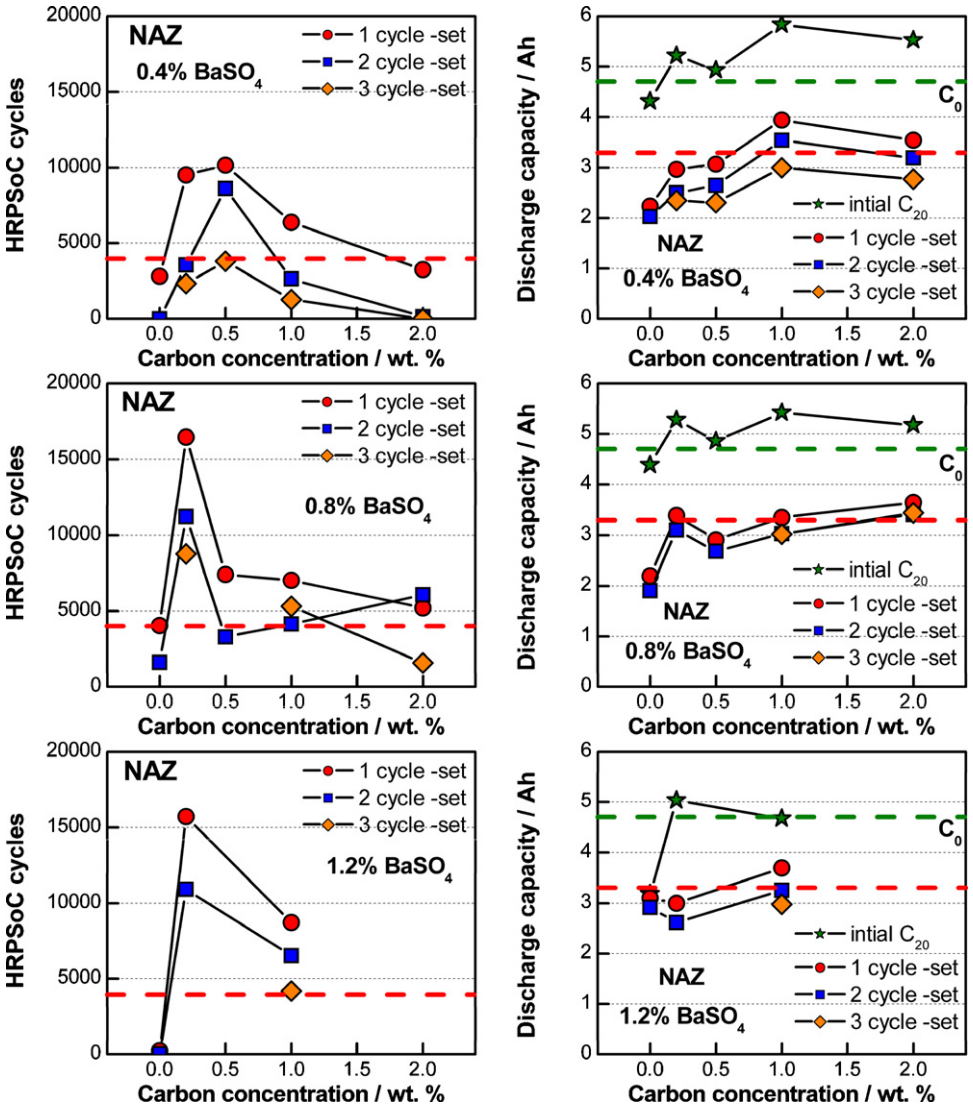

Fig. 12. Influence of Norit AZO activated carbon and $BaSO_4$ concentrations in NAM on the number of completed cycles and on cell capacity for three consecutive HRPSoC cycle sets.

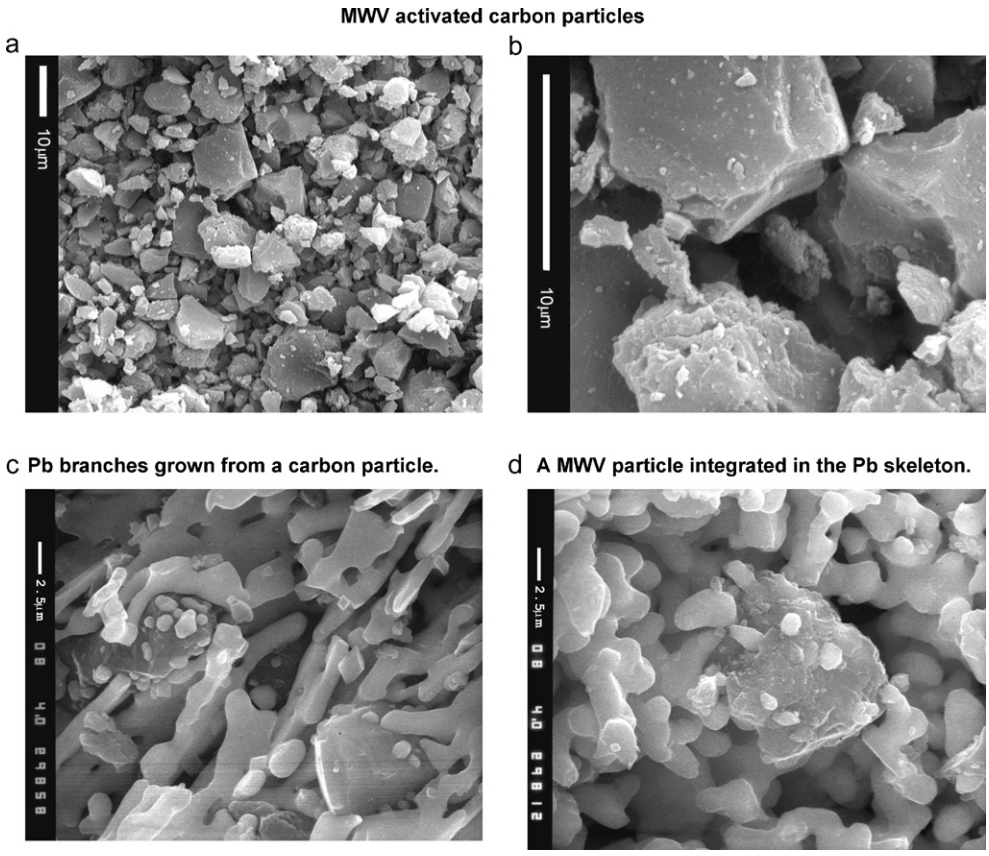

Fig. 13. (a and b) Microstructure of Mead Westvaco purified VW-E-105 activated carbon particles; (c and d) microstructure of NAM with MWV activated carbon and 0.4 wt.% $BaSO_4$.

inclusions in the Pb active mass. Lead nuclei are formed at many sites on the surface of the big carbon particles, but these nuclei grow very slowly. Apparently, the parallel mechanism of reduction of Pb^{2+} ions to Pb proceeds but at a very low rate on the carbon surface. This is, probably, due to the low affinity of lead towards carbon as well as to the higher ohmic resistance of the lead/carbon contact. If this affinity were high, the lead nuclei formed on the carbon surface would grow rapidly and connect to the NAM skeleton.

Fig. 12 illustrates the influence of NAZ activated carbon and $BaSO_4$ content on the number of HRPSoC cycles and on cell capacity. A well expressed peak in the number of completed cycles within the first cycle set is observed at the low carbon concentrations from 0.2 wt.% to 0.5 wt.%. The height of this maximum is influenced by the concentration of $BaSO_4$. On increase of the latter's content in NAM, this maximum shifts from 0.5 wt.% to 0.2 wt.% NAZ concentration and the number of completed cycles grows from 10,000 to 16,000 cycles during the first cycle set. After this maximum, further increase of the NAZ activated carbon content reduces the number of completed cycles per cycle set.

Fig. 12 shows also the initial (C_{20}) capacities and the discharge capacities of the cells after each cycle set. All cells have initial capacity higher than the nominal value (C_0), which then declines down to the end-of-life limit value within the first cycle set already. This tendency is observed even with the cells with low carbon and $BaSO_4$ concentrations.

3.5.2. *Effects of Mead Westvaco activated carbon*

The SEM images in Fig. 13 show the microstructure of Mead Westvaco (MWV) purified WV-E 105 activated carbon particles (upper two pictures) and their incorporation in the lead skeleton of NAM (lower two pictures). These carbon particles are sized from tens of micrometers down to sub-micron dimensions. The latter particles are probably obtained by grinding of the initial carbon mass. The lower two photos in the figure evidence that MWV carbon particles are integrated in the lead skeleton and have become part of it. Lead nuclei have formed on the surface of the carbon particles and grow to form new branches, which are included in the lead skeleton (Fig. 13c). Due to the high affinity of carbon to lead, high currents flow through this contact and the electrochemical reduction $Pb^{2+} + 2e^- \rightarrow Pb$ proceeds at a high rate. Thus carbon particles represent a component of the lead skeleton and the charge reactions proceed on the surfaces of both phases via the parallel mechanism of charge (Fig. 13d).

Fig. 14 shows the number of completed HRPSoC cycles versus the content of MWV activated carbon in NAM at the three different concentrations of $BaSO_4$. Cells with 0.4 wt.% or 0.8 wt.% $BaSO_4$ in NAM complete increasing number of cycles with increase of the MWV carbon content. At the higher $BaSO_4$ loading level (1.2 wt.%), the best cycleability is observed at 1.0 wt.% MWV content and then it declines rapidly with further increase of the carbon load in NAM.

The number of completed cycles by cells with MWV activated carbon in NAM declines considerably after each cycle set. Most probably, this carbon type is oxidized more readily by the evolved oxygen than the other carbon materials. The oxidized carbon particles upset the electro-conductive system of the NAM skeleton and hence the cell completes less cycles during the subsequent cycle set. This effect will depend on the positions occupied by carbon particles in the skeleton and on the way they are connected to the lead particles.

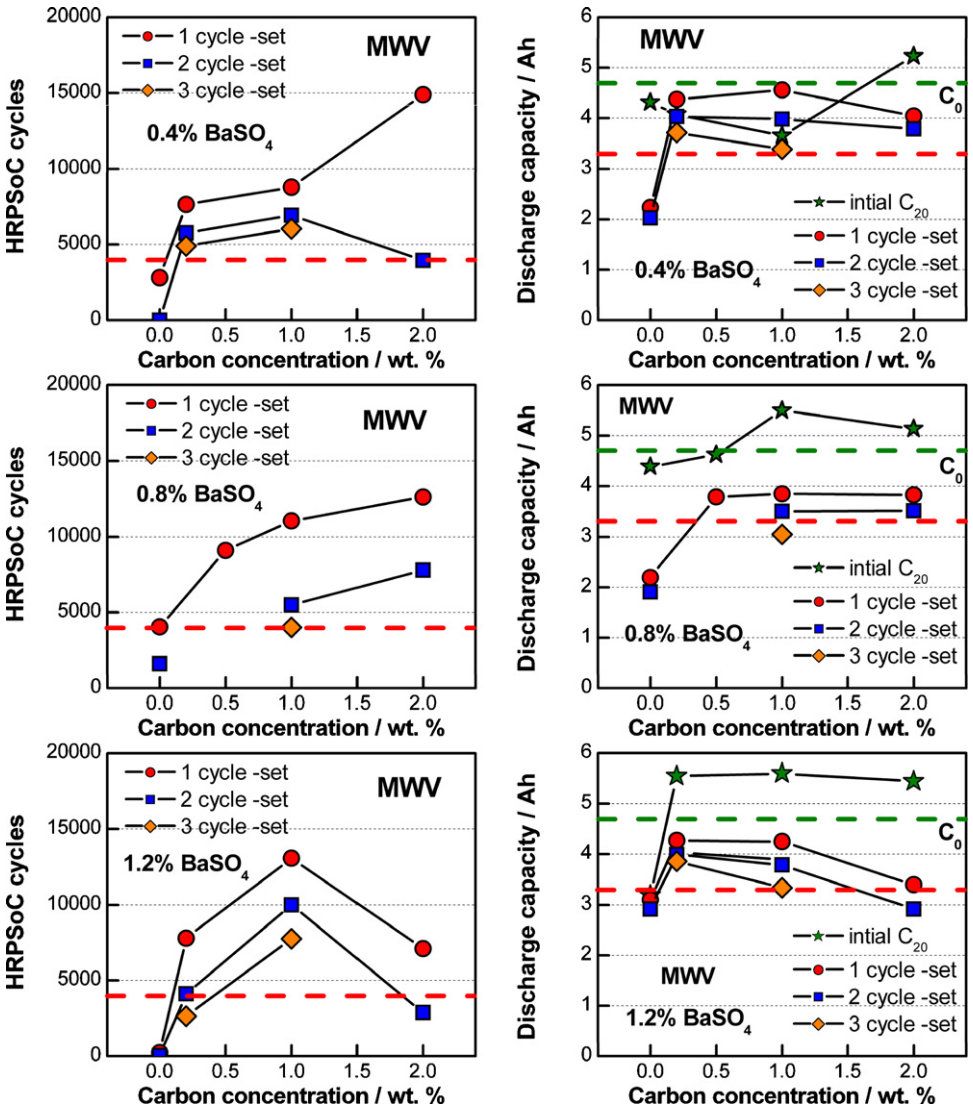

Fig. 14. Influence of MWV Purified VW-E-105 activated carbon and $BaSO_4$ concentrations in NAM on the number of completed cycles and on cell capacity for three consecutive HRPSoC cycle sets.

The initial capacities and the discharge capacities of the cells after each cycle set are also presented in Fig. 14 as a function of MWV carbon and $BaSO_4$ content in NAM. All cells yield initial capacity close to or higher than the nominal capacity, especially at 0.8 wt.% and 1.2 wt.% $BaSO_4$ loading levels. The discharge capacity of the cells after the HRPSoC cycling declines significantly as compared to the initial capacity values, but remains above the end-of-life limit of 70% of the nominal capacity. A relatively small decrease in cell discharge capacity is observed after each cycle set because the discharge current is much lower than the current during the HRPSoC cycling.

3.5.3. *Effects of TDA activated carbon*

The microstructure of TDA-Research SO-15A activated carbon particles (upper two SEM micrographs) and the sites of their inclusion in the lead skeleton of NAM (middle and lower two SEM images) are illustrated in Fig. 15. The TDA activated carbon particles have micron or sub-micron dimensions (Fig. 15a and b). The micrographs of NAM evidence clearly that the carbon particles have become an ingredient part of the lead skeleton and participate in its build-up. The middle right picture (Fig. 15d) features lead branches grown from one big carbon particle. The lower two photos (Fig. 15e and f) show numerous lead nuclei formed on the surface of the carbon particle that grow and tend to cover almost completely the latter' surface. These micrographs demonstrate clearly that there exists a great affinity between carbon and lead particles, and that they can form together a lead skeleton.

Let us now see how does the TDA activated carbon type affect the HRPSoC cycleability and the capacity of the cells. Fig. 16 presents the obtained HRPSoC cycling results for cells with various quantities of TDA activated carbon in the negative plates at three different concentrations of $BaSO_4$.

Increase of TDA carbon content leads to an increase in the number of completed cycles per cycle set at all three concentrations of $BaSO_4$. At 2.0 wt.% TDA level, the cells complete 10,000 cycles per cycle set, with only a small decrease in the number of completed cycles during each subsequent cycle set, which promises a much longer cycle life of cells with this loading level of the TDA activated carbon in NAM.

It is worth noticing that the difference in completed cycles between the first and the second cycle sets is much smaller than that between the second and the third cycle sets for cells with up

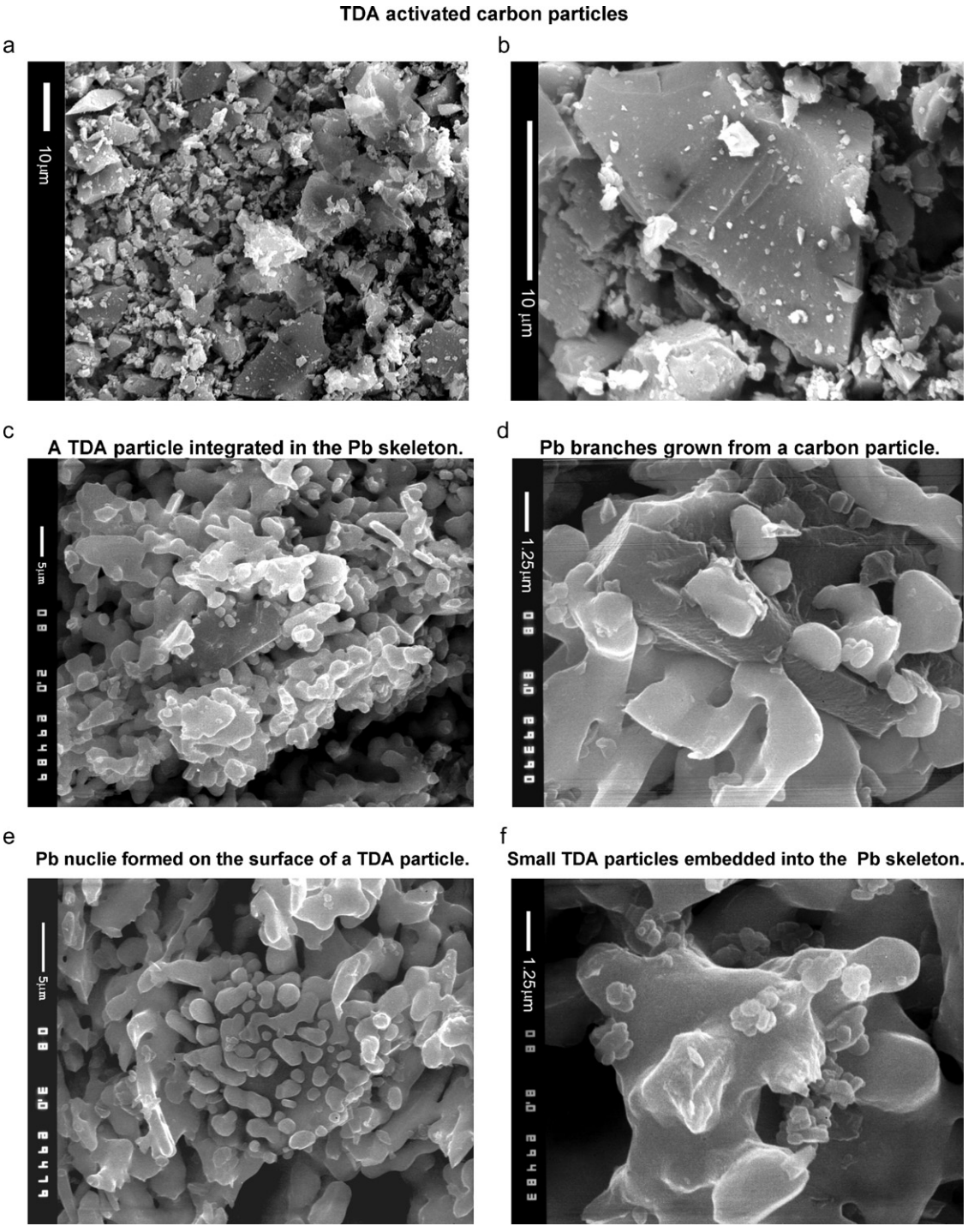

Fig. 15. (a and b) Microstructure of TDA SO-15A activated carbon particles; (c–f) microstructure of NAM with TDA activated carbon and $BaSO_4$.

to 1.0 wt.% TDA carbon in NAM. The situation changes when the content of TDA is increased to 2.0 wt.% for the cells with 0.8 wt.% $BaSO_4$. These variations may be related to the different locations of the TDA particles in the NAM skeleton as well as to their ability to resist to the oxygen attack. The observed increase in the number of completed HRPSoC cycles with increase of the TDA carbon content suggests that this carbon type has a very high affinity to lead while the rate of its oxidation is not very high.

Fig. 16 shows also the changes in initial capacity and discharge cell capacity after each subsequent cycle set as a function of TDA activated carbon content in NAM for the three $BaSO_4$ concentrations. An analogous trend is observed here again, namely the cell capacity increases with increase of the TDA content in NAM. Besides, at 1.0 and 2.0 wt.% carbon loads the capacity decreases but very slightly after each subsequent cycle set. It could be presumed that TDA activated carbon is more resistant to oxidation by the oxygen evolved by the reactions of the closed oxygen cycle.

Further investigations should be performed with TDA activated carbon loads higher than 2.0 wt.%.

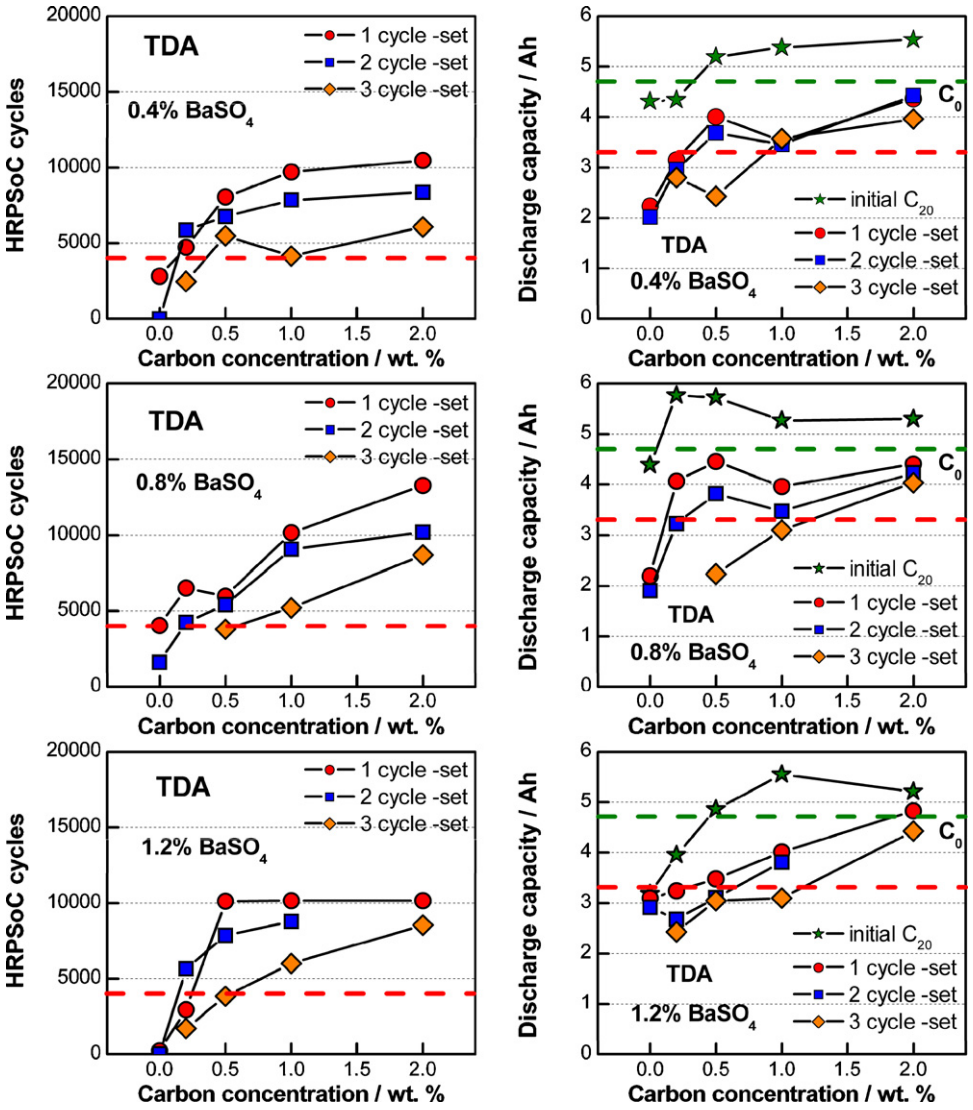

Fig. 16. Influence of TDA SO-15A activated carbon and $BaSO_4$ concentrations in NAM on the number of completed cycles and on cell capacity for three consecutive HRPSoC cycle sets.

4. Conclusions

4.1. A new lead–carbon electrode in the lead-acid battery

The above discussed experimental results suggest that the lead electrode in the lead-acid battery may possibly transform into a lead–carbon electrode. For this to happen in practice, the carbon type used as an additive to NAM should have high affinity to lead. If this is the case, another factor of primary importance is the amount and the size of the carbon particles. If carbon black particles of nano-sizes (i.e. much smaller than the diameter of the NAM skeleton branches) are used, as for example Printex carbon black (PRU), depending on their concentration in NAM they may be incorporated into the bulk of the lead skeleton branches of NAM or may be adsorbed on the surface of the lead phase. When PRU carbon black is added to NAM in concentrations from 0.2 wt.% to 0.5 wt.%, the negative plates have high electrical performance. At low concentration of PRU carbon black particles in the negative active material, they will be pushed to the surface of the NAM during formation and will thus contribute to the growth of the electrochemically active surface of NAM and eventually to improving the charge acceptance of the negative plates. At loading levels higher than 0.5 wt.%, the PRU carbon black particles of sub-micron sizes are incorporated into the bulk of the lead phase. The electrical parameters of NAM are impaired substantially.

When the dimensions of activated carbon particles are of the order of tens of micrometers (i.e. a size larger than the cross-section of NAM lead branches) and have high affinity to lead (as for example TDA or MWV activated carbons), the carbon particles get integrated into the lead skeleton and become integral components of this skeleton. During formation, lead nuclei will form on the surface of these activated carbon particles and will grow into new branches, thus forming a lead–carbon active mass. Activated carbon particles (TDA and MWV) have high surface area and microporous structure. When their pores are filled with water, they acquire the properties of a super-capacitor. Water and H^+ ions penetrate into the carbon pores. During charging, these carbon particles act as super-capacitors. Electric charges are concentrated in them and then they are distributed along the branches of the lead skeleton with the lowest ohmic resistance. This makes the lead skeleton a more dynamic electric system, which will be charged and discharged easier, which will improve the charge acceptance of the negative plates.

When the closed oxygen cycle operates in the cells, the lead–carbon active mass structure is subjected to oxygen attack. The evolved oxygen oxidizes some of the carbon particles and thus upsets the electro-conductive system of the NAM skeleton, which eventually impairs the charge acceptance of the negative plates and shortens the cycle life of the cells. Hence, a further criterion in the selection of appropriate carbon additive(s) to the negative active material should be their ability to resist to oxygen attack, which would guarantee stable electrical performance and long cycle life of the battery in the HRPSoC cycling duty. Thus, the charge acceptance of the lead–carbon electrode of the lead-acid battery may be improved and the latter may gain larger share of the hybrid electric vehicle batteries market.

Acknowledgements

The authors acknowledge with gratitude the financial support provided by the Advanced Lead-Acid Battery Consortium (ALABC Project No. 1012G). We want to express our special thanks to Dr. P. Moseley and Dr. D. Prengaman for encouraging the present investigation and to Dr. K. Bullock for the very useful discussion.

References

[1] Nakamura, M. Shiomi, K. Takahashi, M. Tsubota, J. Power Sources 59 (1996) 153.
[2] M. Shiomi, T. Funato, K. Nakamura, K. Takahashi, M. Tsubota, J. Power Sources 64 (1997) 147.
[3] P.T. Moseley, R.F. Nelson, A.F. Hollenkamp, J. Power Sources 157 (2006) 3.
[4] A.F. Hollenkamp, W.G.A. Baldsing, S. Lau, O.V. Lim, R.H. Newnham, D.A.J. Rand, J.M. Rosalie, D.G. Vella, L.H. Vu, ALABC Project N1.2, Final Report 2002, Advanced Lead-Acid Battery Consortium, Research Triangle Park, NC, USA, 2002.
[5] P.T. Moseley, J. Power Sources 191 (2009) 134.
[6] L.T. Lam, C.G. Phyland, D.A.J. Rand, D.G. Vella, L.H. Vu, ALABC Project N3.1, Final Report 2002, Advanced Lead-Acid Battery Consortium, Research Triangle Park, NC, USA, 2002.
[7] M. Fernandez, J. Valenciano, F. Trinidad, N. Munos, J. Power Sources 195 (2010) 4458.
[8] D.P. Boden, D.V. Loosemore, M.A. Spense, T.D. Wojcinski, J. Power Sources 195 (2010) 4470.
[9] K.R. Bullock, J. Power Sources 195 (2010) 4513.
[10] D. Pavlov, T. Rogachev, P. Nikolov, G. Petkova, J. Power Sources 191 (2009) 58.
[11] D. Pavlov, P. Nikolov, T. Rogachev, J. Power Sources 195 (2010) 4444.